Supplementary Information for

Oligomeric Aβ in the monkey brain affects synaptic integrity and induces accelerated cortical aging

Danielle Beckman, Sean Ott, Kristine Donis-Cox, William G. Janssen, Eliza Bliss-Moreau, Peter H. Rudebeck, Mark G. Baxter, John H. Morrison*

*Corresponding author:

John H. Morrison, California National Primate Research Center, UC Davis, Davis, CA 95616, USA; Phone: (530)752-7059; E-mail: jhmorrison@ucdavis.edu

This PDF file includes:

www.pnas.org/cgi/doi/10.1073/pnas.1902301116

Fig. S1.

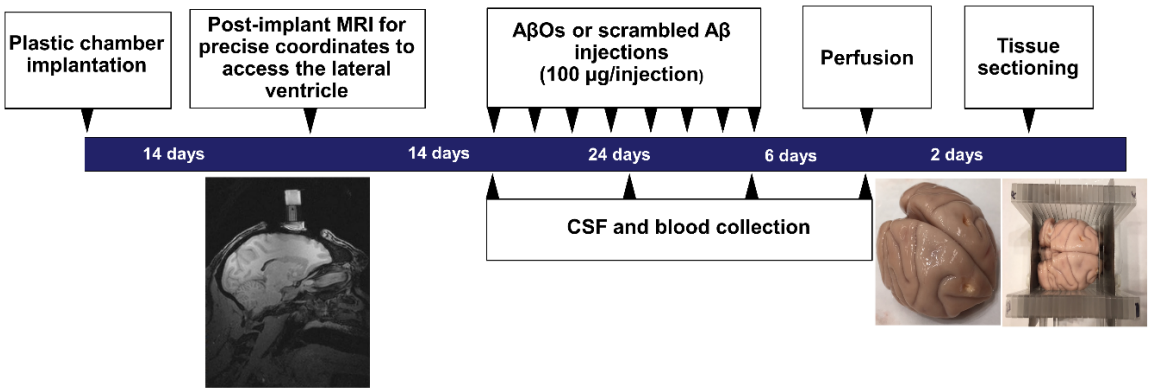

Time course of Aβ oligomer (AβO) or scrambled Aβ injection. 6 monkeys received a plastic chamber implantation and following 2 weeks of recovery, an MRI was performed on each animal to obtain the precise coordinates for accessing the lateral ventricle. After 2 more weeks of recovery, 4 animals were injected with freshly prepared and fully characterized AβOs and 2 animals were injected with the scrambled Aβ preparation. The delivery rate of the infusion was carefully monitored to ensure the total concentration of 100 µg of peptide was infused inside the lateral ventricle. Injections were performed once per day, every 3 days, for 24 days. Perfusion of the animals was performed 6 days after the last infusion. CSF and blood were collected from the animals prior to the first injection, approximately every ten days during the injection period and immediately before perfusion. Saline perfused brains were fixed for 48 hours in PFA 4% with 0.125% glutaraldehyde. After fixation, brains were washed with PBS and sectioned for immunohistochemical analyses.

Fig. S2.

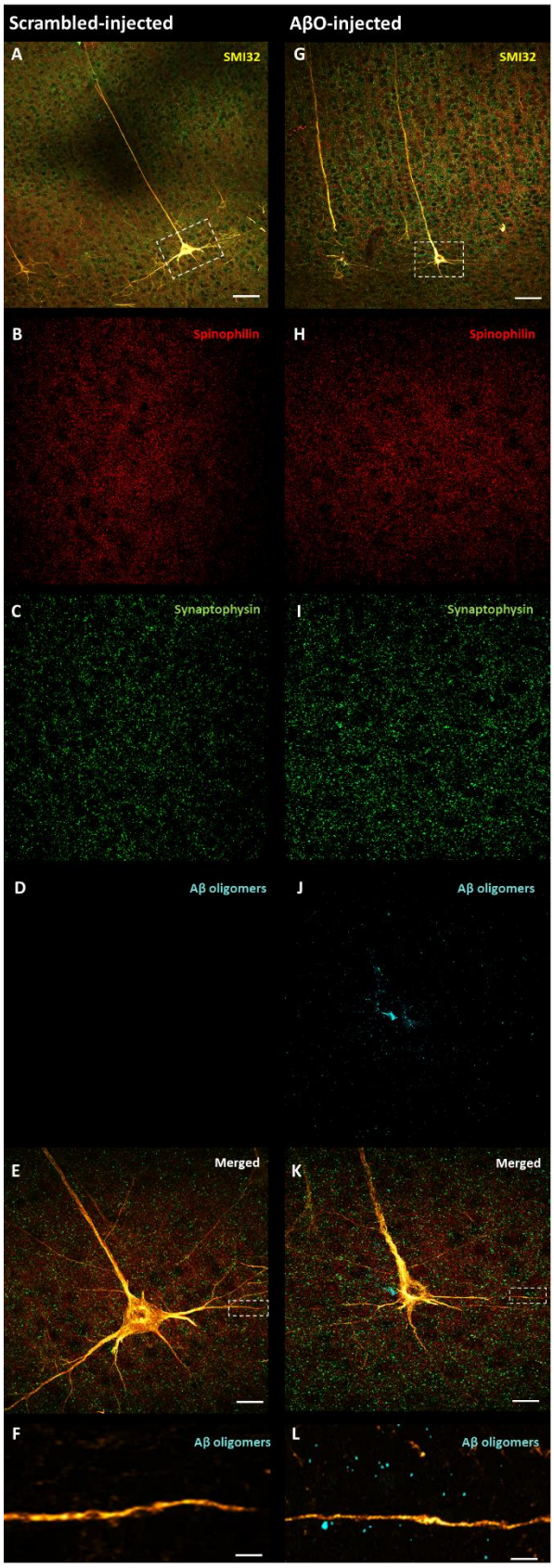

No AβO puncta staining is detected in the scrambled Aβ injected animals. Immunohistochemistry in the dorsolateral prefrontal cortex (DLPFC) layer III shows pyramidal neurons stained with SMI32 (A, G), PSD95 (B, H), synaptophysin (C, I) and merged images (E, K). In F and L, a higher magnification of one of the dendritic segments shows abundant oligomeric Aβ staining around the segment in the AβO-injected animal, but not in the scrambled Aβ injected animal. Scale bar: 20 µm, 2 µm (F, L).

Fig. S3.

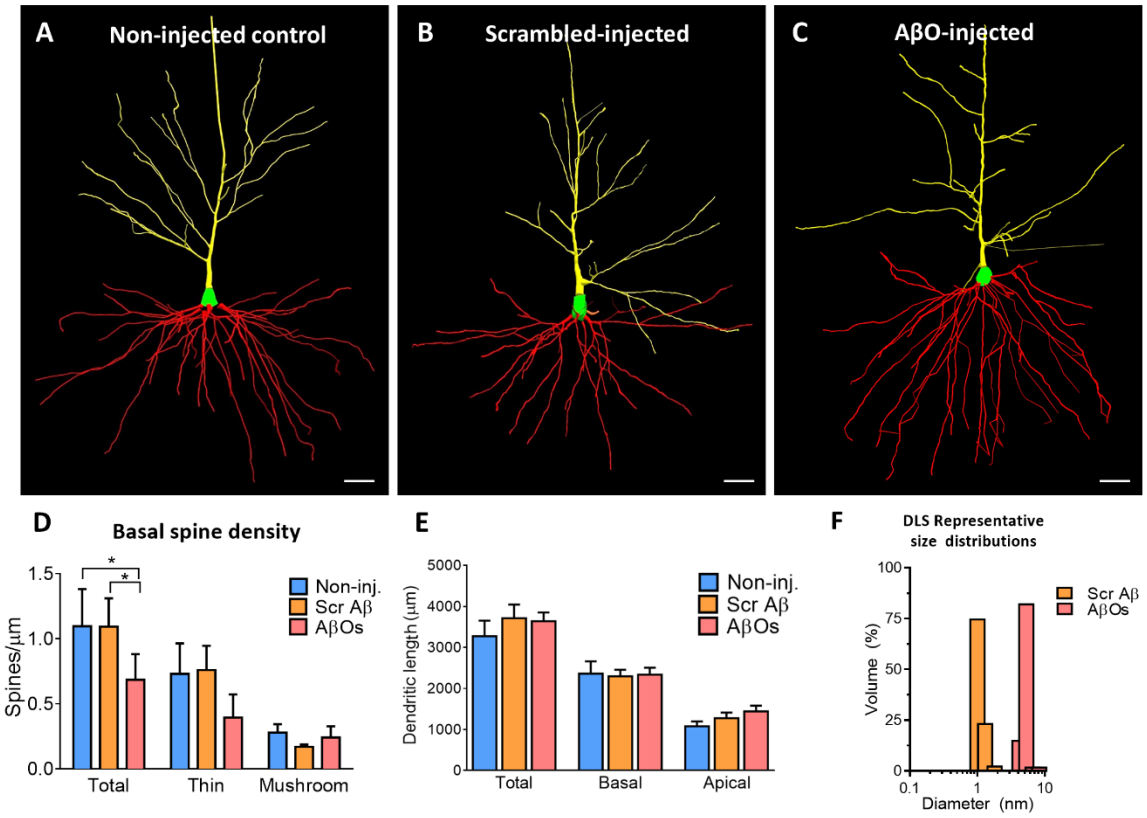

Reduction in basal spine density but no changes in overall dendritic arborization of cortical neurons in Aβ-scrambled or AβO-injected animals. Representative example of 3D reconstructed neurons from (A) non-injected animals, (B) Scrambled Aβ injected animals and AβO-injected animals. (D) Spine density of basal segments shows a reduction in the total number of spines only in the AβO-injected animals. (E) Quantification of dendritic length of the analyzed neurons shows no differences among the groups. (E) AβOs and scrambled Aβ were freshly prepared and characterized before every injection. The Dynamic light scattering (DLS) technique was used to measure the size distribution profile of the Aβ species preparations. AβOs average diameter was 4.14 nm and scrambled Aβ average diameter was 1.8 nm (monomers). Scale bar: 20 µm. *p<0.05,

Fig. S4.

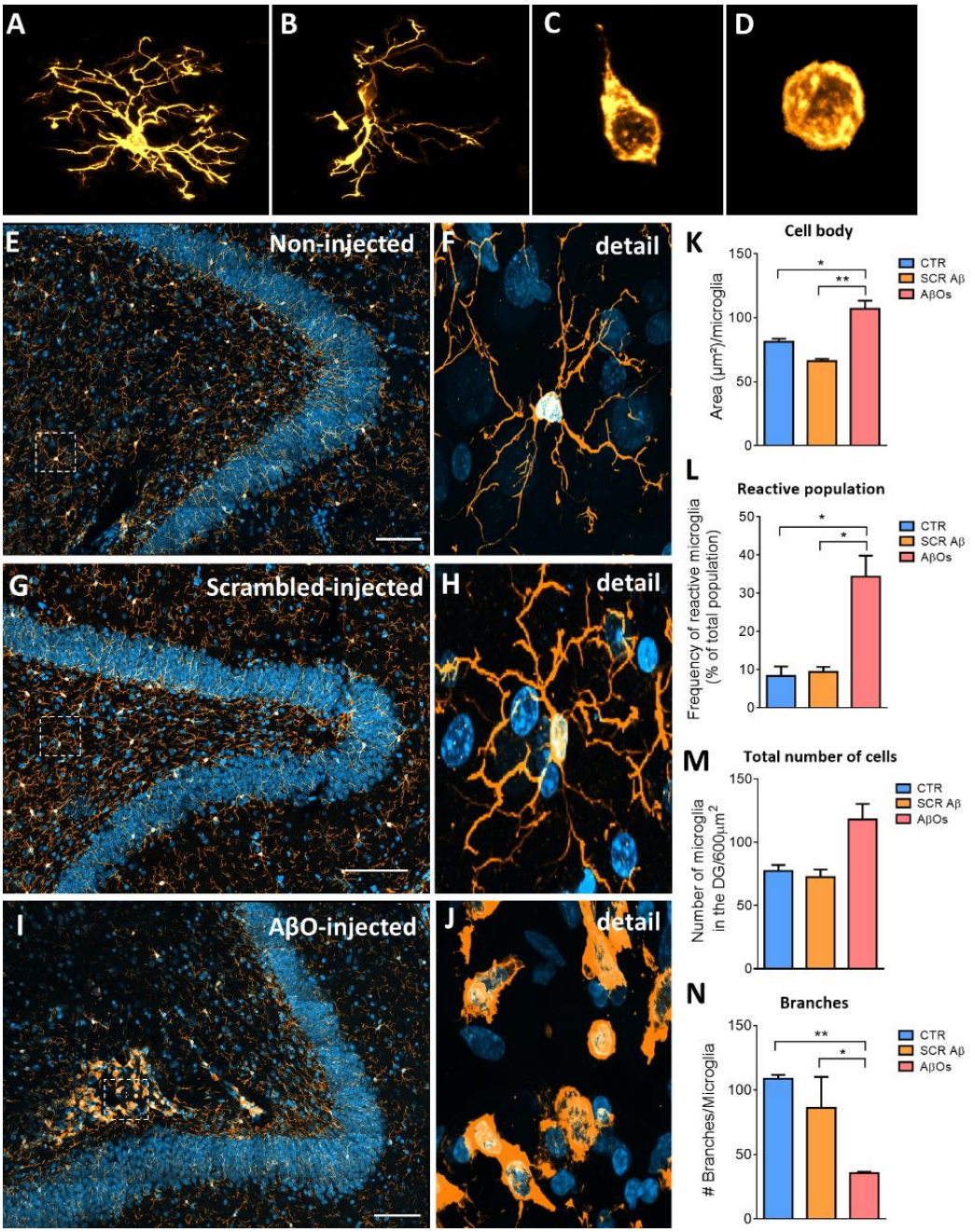

AβO injection induces robust microgliosis and neuroinflammation in the hippocampus. Representative z-stacks of microglia (IBA-1) showing diverse activation states: physiological/resting (A), intermediate (B), amoeboid (C) and round (D). The last two are considered reactive microglia states. (E, G, I) Representative z-stacks for microglia

stained for IBA-1 showing profound morphologic changes and microgliosis induced by AβOs in the CA3/hilus of the hippocampus. Microglia from AβO-injected animals are increased in size (K), with an increase in microglia present of more than 4x in AβO-infused monkeys (L). The total number of microglia is increased in the DG (M) with a decrease in the number of branches (N), indicating extensive microgliosis occurring in the AβO-injected animals. *$p<0.05$, **$p< 0.01$ one-way ANOVA, Tukey's post-hoc test. Scale bar: 100 μm.

Fig. S5.

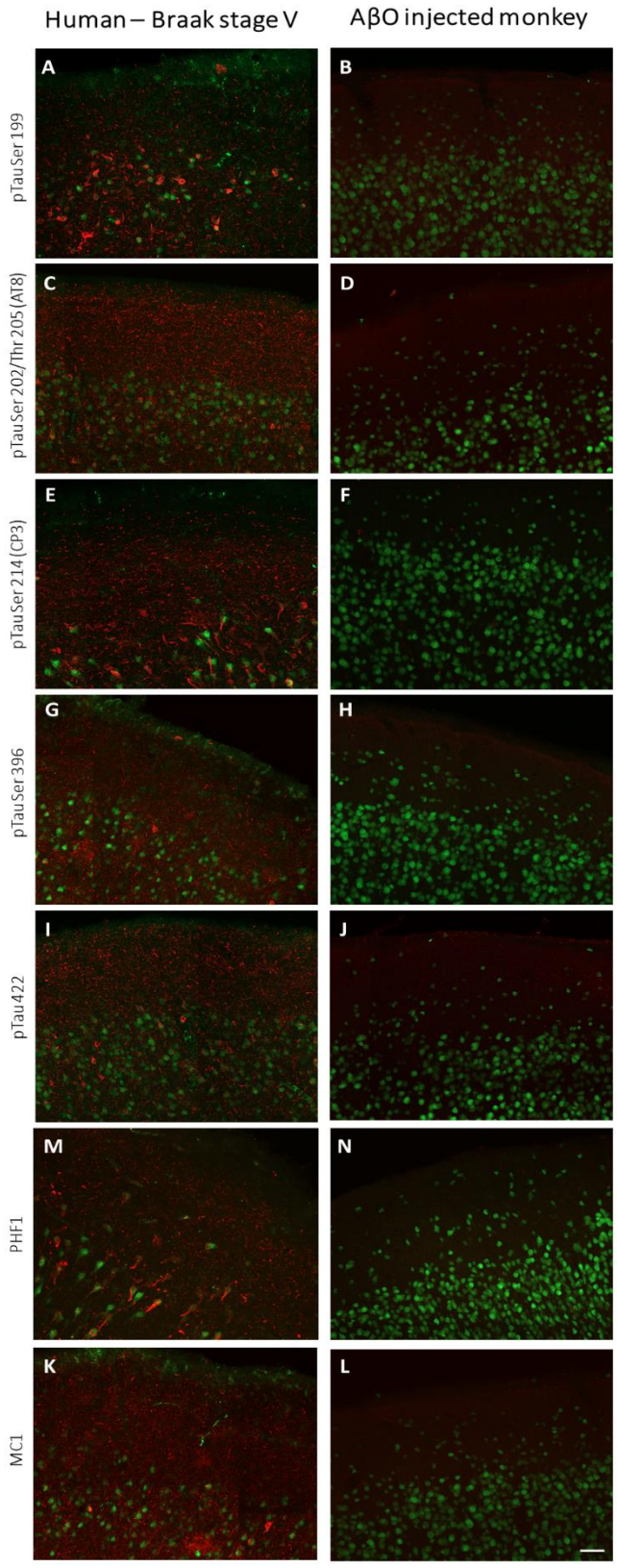

No detection of tau pathology in entorhinal cortex (ERC - layer II) of AβO-injected animals. Representative images of immunohistochemistry in the ERC – layer II of a human AD case and AβO-injected animals. Antibodies against different tau phosphorylation states were used: pTau Ser 199 (A, B), pTau Ser 202/Thr 205 (C, D), pTau Ser 214 (E, F), pTau Ser 396 (G, H), pTau Ser 422 (I, J), PHF1 (M, N) and the conformation dependent antibody MC1 (K, L). We were able to confirm that no tau-based pathology similar to that observed in human AD ERC was observed with the current protocol of injections over the course of 24 days in AβO -injected animals. Scale bar: 50 µm.

Fig. S6.

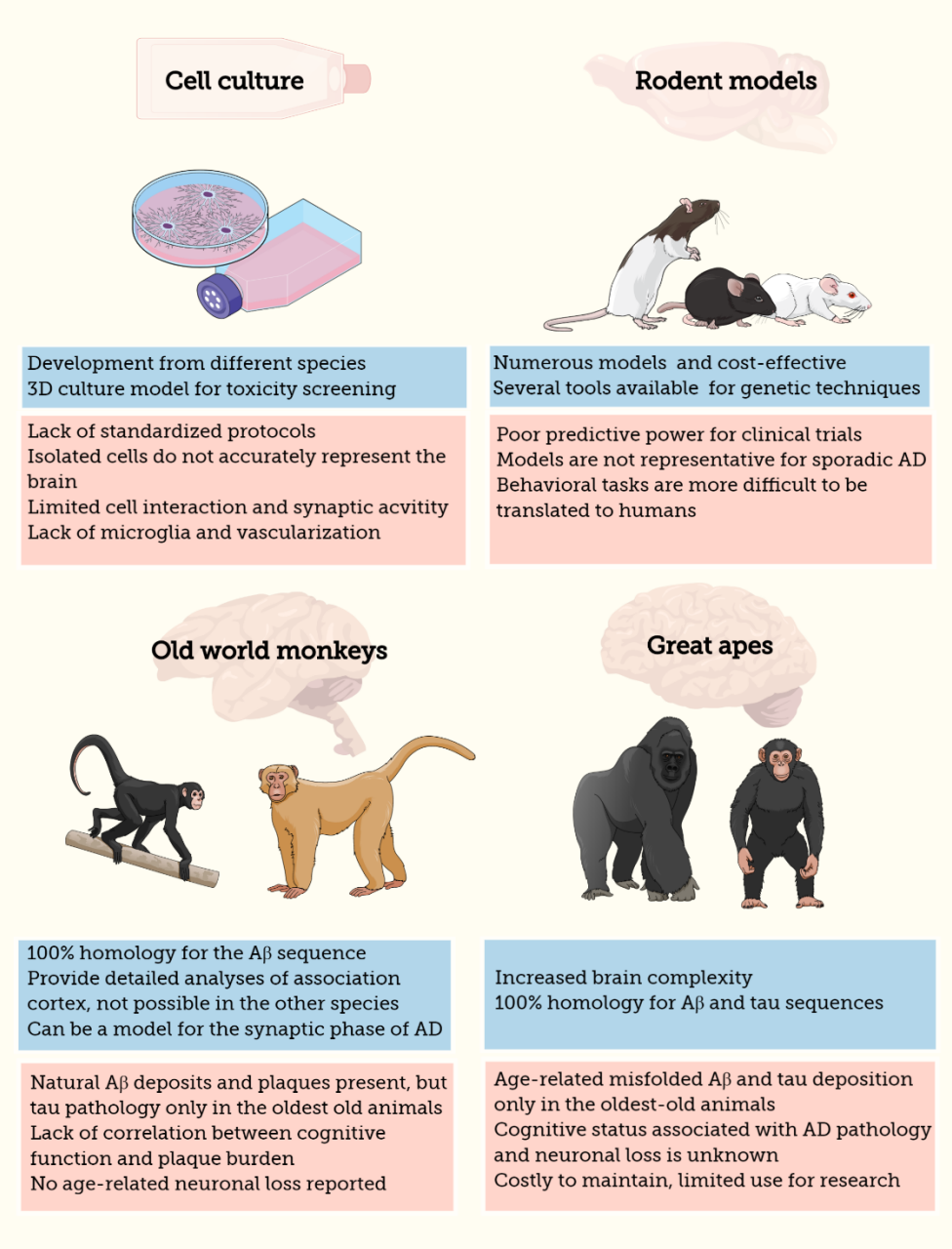

Figure 6: Key advantages and disadvantages of each animal model for Alzheimer's disease. The major animal models used for AD research are based on cell culture models and transgenic mice carrying autosomal mutations in APP, PS1 or PS2 genes. Although substantial advances were made in the development of these models, including 3D cultures

of human neurons and better transgenic animals for tau pathology, these models more accurately reflect early-onset familial Alzheimer's disease (EOAD) which represents less than 5% of AD cases. On the other hand, current models are limited with respect to sporadic late-onset AD (sAD). Non-human primates present several neuropathological markers related to age and degenerative processes, but not necessarily the full extent of AD pathology. Old World monkeys like African green monkeys and rhesus monkeys present extensive accumulation of amyloid plaques with aging, but these do not correlate with cognitive dysfunction and memory loss. On the other hand, they may represent valuable models for studying the early stages of synaptic disruption in the prodromal stage of AD. Although great apes can show markers of AD-like pathology among the oldest-old animals, none of the studies thus far has demonstrated that these animals present the four hallmarks of AD: amyloid plaques, NFTs, neuronal loss, and dementia that correlates with NFTs and degree of neuronal loss. Due to their long-life cycle and limited availability for research, these animals do not represent the best option for translational studies in AD.

Table S1. Details of the human brain samples used in this study.

Clinical diagnose	Age	Sex	Ethnicity	Post mortem delay (H)	Braak stage	Neuropathological diagnose	Brain region analyzed
CTRL	71	M	White	3	2	Low likelihood of AD pathology according to the NIA-Alzheimer's Association CERAD score: 0	DLPFC
CTRL	95	M	White	4	1	Left hippocampal sclerosis; Ischemic brain injury due to small vessel disease. Low likelihood of AD pathology according to the NIA-Alzheimer's Association CERAD score: 0	DLPFC
CTRL	96	F	White	7	2	Ischemic brain injury, microhemorrhage in middle frontal gyrus, mild pallor in parietal deep white matter. Low likelihood of AD pathology according to the NIA-Alzheimer's Association CERAD score: 1	DLPFC
CTRL	84	F	White	-	1	Leptomeningeal carcinomatosis and intraparenchymal metastatic carcinoma Low likelihood of AD pathology according to the NIA-Alzheimer's Association	DLPFC

						CERAD score: 0	
AD	81	M	White	5	6	Neuropathological examination revealed severe Alzheimer's disease pathology, and did not reveal Lewy bodies. CERAD score: 3	DLPFC
AD	90	M	White	13	6	Wide-spread amyloid angiopathy	DLPFC
AD	88	M	White	7	6	Severe Alzheimer's disease pathology. Sparse Lewy bodies in the cingulate gyrus Severe atherosclerosis CERAD score: 3	DLPFC
AD	85	M	-	11	5	CDR 3 MMSE 11	ERC

Table S2: Detailed statistical analysis used in the study

Comparison	Test	Statistic
Figure 1I: Quantification of colocalization puncta	Two-sample unpaired t-test	t(6) = 3.048, p = .0226
Figure 2C: Total spine density (young vs aged)	2-way ANOVA followed by Sidak's multiple comparisons test	Age x Spine Type interaction F(2, 14) = 20.19, p < .0001
		Young vs aged Total t(21) = 4.41, p < .05 Thin t(21) = 4.65, p < .05 Mushroom t(21) = 0.41, p = ns
Figure 2D: Head diameter (young vs aged)	Two-sample unpaired t-test	t(7) = 8.504, p < .0001
Figure 2H: Apical spine density (AβOs)	2-way ANOVA followed by Tukey's multiple comparisons test	Injection (none/scrambled/AβO) x Spine Type interaction F(4, 12) = 4.08, p = 0.0258
		Total spines Non-injected vs AβOs q(18)=4.393, p < .05 Scrambled vs AβOs q(18)=3.696, p < .05 Thin spines Non-injected vs AβOs q(18)=3.777, p < .05 Other comparisons p > .05
Supplementary figure 3D: Basal spine density (AβOs)	2-way ANOVA followed by Tukey's multiple comparisons test	Injection (none/scrambled/AβO) x Spine Type interaction F(4, 12) = 3.438, p = 0.0431
		Total spines Non-injected vs AβOs q(18)=4.177, p < .05 Scrambled vs AβOs q(18)=3.658, p < .05 Other comparisons p > .05
Figure 2I: Spine head diameter (AβOs)	One-way ANOVA followed by Tukey's multiple comparisons test	Injection (none/scrambled/AβO) F(2, 7) = 6.461, p = .0257
		Non-injected vs AβOs q(7) = 4.582, p < .05 Other comparisons p > .05

Figure 3C: Microglia volume (young vs aged)	Two-sample unpaired t-test	t(5) = 2.665, p = .0446
Figure 3H: Microglia volume (AβOs)	One-way ANOVA	Injection (none/scrambled/AβO) F(2, 6) = 4.44, p = .0656
Figure 3I: Colocalization of PSD95 in microglia	One-way ANOVA followed by Tukey's multiple comparisons test	Injection (none/scrambled/AβO) F(2, 7) = 5.754, p = .0333
		Non-injected vs AβOs q(7) = 4.239, p < .05 Other comparisons p > .05
Figure 3J: Colocalization of C1q in microglia	One-way ANOVA	Injection (none/scrambled/AβO) F(2, 7) = 1.834, p = .23
Figure 3K: Colocalization of synaptophysin in microglia	One-way ANOVA	Injection (none/scrambled/AβO) F(2, 7) = 0.28, p = .76
Supplementary figure 4K (cell body area)	One-way ANOVA followed by Tukey's multiple comparison test	Injection (none/scrambled/AβO) effect, F(2, 6) = 14.43, p = 0.0051
Supplementary figure 4L (number of microglia)	One-way ANOVA followed by Tukey's multiple comparison test	Injection (none/scrambled/AβO) effect, F(2, 6) = 6.067, p = 0.0362
Supplementary figure 4M (frequency of amoeboid)	One-way ANOVA followed by Tukey's multiple comparison test	Injection (none/scrambled/AβO) effect, F(2, 6) = 10.98, p = 0.0099
Supplementary figure 4N (branches/microglia)	One-way ANOVA followed by Tukey's multiple comparison test	Injection (none/scrambled/AβO) effect, F(2, 6) = 23.86, p = 0.0014
Figure 4A: AβOs ELISA	2-way ANOVA followed by Sidak's multiple comparisons test	Injection (scrambled / AβO) x time interaction F(3, 12) = 8.758, p = .0024 Injection main effect F(1, 4) = 20.47, p = .0106
Figure 4B: Aβ1-42 ELISA	2-way ANOVA followed by Sidak's multiple comparisons test	Injection (scrambled / AβO) x time interaction F(3, 12) = 5.702, p = .0116

		Injection main effect F(1, 4) = 14.83, p = .0183
Figure 4C: Aβ1-40 ELISA	2-way ANOVA followed by Sidak's multiple comparisons test	Injection (scrambled / AβO) x time interaction F(3, 12) = 1.289, p = .3228 Injection main effect F(1, 4) = 0.14, p = .727
Figure 4D: Neurofilament light ELISA	2-way ANOVA followed by Sidak's multiple comparisons test	Injection (scrambled / AβO) x time interaction F(3, 12) = 0.44, p = .728 Injection main effect F(1, 4) = 0.39, p = .565
Figure 4E: TNF alpha ELISA	2-way ANOVA followed by Sidak's multiple comparisons test	Injection (scrambled / AβO) x time interaction F(3, 12) = 3.803, p = .0398 Injection main effect F(1, 4) = 3.714, p = .1262
Figure 4F: IL-6 ELISA	2-way ANOVA followed by Sidak's multiple comparisons test	Injection (scrambled / AβO) x time interaction F(3, 12) = 13.26, p = .0004 Injection main effect F(1, 4) = 4.613, p = .0982
Figure 4G: Tau pS199 ELISA	2-way ANOVA followed by Sidak's multiple comparisons test	Injection (scrambled / AβO) x time interaction F(3, 12) = 1.036, p = .4118 Injection main effect F(1, 4) = .0067, p = .939
Figure 4H: Tau pS231 ELISA	2-way ANOVA followed by Sidak's multiple comparisons test	Injection (scrambled / AβO) x time interaction F(3, 12) = 0.2776, p = .8405 Injection main effect F(1, 4) = 0.036, p = .858
Figure 4I: Tau pS396 ELISA	2-way ANOVA followed by Sidak's multiple comparisons test	Injection (scrambled / AβO) x time interaction F(3, 12) = 0.4375, p = .7303 Injection main effect F(1, 4) = 1.114, p = .3507
Figure 4J: Total tau ELISA	2-way ANOVA followed by Sidak's multiple comparisons test	Injection (scrambled / AβO) x time interaction F(3, 12) = 0.3089, p = .8186 Injection main effect F(1, 4) = 0.0045, p = .95

Supplementary Materials and Methods

Human brain samples: 4 confirmed AD cases and 4 aged-matched controls DLPFC samples were obtained from the UC Davis Alzheimer's Disease Center, grant: P30-AG010129, provided by Dr. Lee-Way Jin. An ERC sample from one confirmed AD case was kindly provided by Dr. Patrick Hof. Please see supplementary table 1 for details of each patient's case.

Monkey surgery: Under full aseptic conditions monkeys were implanted with a plastic chamber (Crist Instruments, MD) that allowed access to the dural surface. Monkeys were intubated, placed in a stereotaxic frame, and maintained on isoflurane anesthesia (1.5%, to effect). A craniotomy was made corresponding in size to the inner diameter of an MRI-compatible plastic infusion cylinder (Crist Instruments), centered 20-25 mm anterior to the interaural plane. The cylinder was fixed to the skull with titanium screws (Veterinary Orthopedic Implants) and a small amount of dental acrylic (Orthojet), and the galea and skin were then closed around the implant.

MRI: Post-implant MRI scans were conducted to obtain precise coordinates for placement of injections into the lateral ventricles. At the time of the scan, a grid was placed into the chamber filled with dilute gadolinium. Infusion needles and cannula were custom-made for each animal using the measurements for the coordinates obtained from the MRI.

AβO and scrambled Aβ infusions: Animals were lightly sedated with ketamine/dexmedetomidine and a sterile grid was placed into the chamber and secured in place being careful to use the exact orientation from the MRI scan. The syringe was attached to the sterile infusion needle assembly and the line between the needle and the syringe hub was allowed to fill with the infusion material from the syringe until a tiny bead

was observed at the tip of the syringe. This was done to avoid injecting air into the ventricles. The infusion material was delivered at a rate of 25 microliters every 30 seconds. After completion, a sterile cap was replaced on the chamber and the animal was given atipamezole and monitored during recovery.

CSF collection: CSF was collected via cisterna magna using standard operating procedures by clinical staff following administration of intramuscular ketamine and dexmedetomidine for immobilization, anesthesia and analgesia. Following hair clipping and sterile field preparation of the base of the skull and dorsal neck, a 23-gauge spinal needle was inserted into the subarachnoid space of the cisterna magna. Approximately 1 ml of CSF was withdrawn through the placed needle using a sterile syringe. The collected CSF was immediately transferred to a cryo tube and flash frozen on dry ice and stored at -80°C. Animals were reversed with intramuscular atipamazole and given injectable ketoprofen for additional analgesia support and recovered.

Perfusion and tissue preparation: All monkeys were deeply anesthetized with ketamine (25 mg/kg) and pentobarbital (20–35 mg/kg, i.v.), intubated, and mechanically ventilated. The chest was opened to expose the heart and heparin was injected into the left ventricle to facilitate vasodilation. The descending aorta was clamped immediately following intubation, and the monkeys were perfused transcardially with warm 0.9 % saline for 5 min followed by cold 0.9% saline for approximately 5-7 min at a rate of 220 ml/min. After perfusion, the brain was removed from the skull and dissected into standardized blocks. Samples for microscopy were immersed in fixative (4% paraformaldehyde with 0.125% glutaraldehyde) for 48 hours before being rinsed in buffer and processed. Frontal and temporal blocks were cut serially on a vibratome (Leica) in 400 µm-thick sections (for

intracellular injection of A568; Invitrogen) or 50 µm-thick sections for fluorescence confocal microscopy.

ELISAs: An ELISA for AβO detection was done as previously described (1, 2) using the monoclonal oligomer specific NAB61 antibody (provided by Dr. Virginia Lee). $A\beta_{1-42}$, $A\beta_{1-40}$, tTau, p-tau Ser199, p-tau Ser231, p-tau Ser396 (Invitrogen), TNF-α, IL-6 (Abcam) and neurofilament-light (Uman Diagnostics) ELISA assays were performed according to each kit's manufacturer's instructions, after sample dilution optimization.

AβO characterization by dynamic light scattering: Particle size analysis of the Aβ solutions were carried out for every preparation prior to injections using dynamic light scattering (DLS) with a Brookhaven 90Plus instrument that monitors scattered light at 90° to the excitation. The samples were centrifuged at 14000xg to remove the large amorphous aggregates just prior to measurement. Measurements were made at sequential dilutions from the undiluted sample of 5µM to 1:2, 1:4, 1:10, 1:100 dilution factors. The average hydrodynamic radius was calculated using the ZetaPlus Particle Sizing Software Version 3.57 (Brookhaven Instruments).

Microscopy and image analysis:

• *Quantitative analyses of spine density and spine morphology:* Intracellular injection of layer III pyramidal cells with alexa 568 and quantitative analysis was performed according to methods previously described (3, 4). Dendritic segments were chosen in a systematic random fashion for branching and spine analysis. A total of 20 apical and 20 basal segments were acquired for each experimental condition, in a total of 6-10 neurons analyzed per experimental group. Photomicrographs of the neurons and segments were made using a Zeiss LSM 800 microscope with Airyscan. After acquisition, neurons and segments were

exported to Neurolucida 360 (MBF Bioscience) for 3D reconstruction and spine analysis. Data was then imported into Matlab for spines classification into thin and mushroom types based on categories previously established in our lab (4).

• *Synaptic markers and AβO puncta colocalization:* For each animal, 5 30-micron apical segments were analyzed from 5-8 neurons positive for SMI32 in the DLPFC of the monkeys in a blinded fashion at 63x using a Zeiss LSM 800 microscope. Data was exported to Imaris software (Bitplane) for 3D reconstruction of the segments and analysis of puncta staining within 2 µm of distance from the segment. After isolation of all puncta around the segment, positive puncta colocalization was considered between AβO and PSD95 or AβO and synaptophysin when the distance between two puncta was 1 µm. Quantification of the data was made comparing all AβO colocalizing with PSD95 and all AβO colocalizing with synaptophysin in a 2 µm distance of one apical segment with a size of 30 µm. 30 - 40 segments were analyzed per animal.

• *Microglia morphology and quantification:* For microglia engulfment analysis in the DLPFC, 20 microglia in a blinded fashion were selected from the DLPFC of each animal. For each microglia, a z-stack at 63x in the Zeiss LSM 800 was collected, and the image was exported to Imaris software to create 3D volume surface rendering of each z-stack. Engulfment quantification was done in a similar way as previously described (5). Briefly, PSD95, synaptophysin 1 and C1q puncta were 3D surface rendered using the same parameters for all the animals. To measure the percentage of engulfment, the volume of internalized puncta (μm^3) was divided by the total volume of microglial cells (μm^3).

For microglia morphology in the DG, three confocal 70 tile 25 µm z-stacks at 63x were made in the Zeiss LSM 800 for the entire DG for each animal using different portions

of the hippocampus. The maximum intensity projection of the IBA-1 staining was converted to a binary image. Only cells presenting the entire cell body were isolated and morphology of the cells was analyzed using the AnalyzeSkeleton plugin (ImageJ software).

References

1. Hölttä M, et al. (2013) Evaluating Amyloid-β Oligomers in Cerebrospinal Fluid as a Biomarker for Alzheimer's Disease. *PLoS One*. doi:10.1371/journal.pone.0066381.
2. Savage MJ, et al. (2014) A sensitive aβ oligomer assay discriminates Alzheimer's and aged control cerebrospinal fluid. *J Neurosci* 34(8):2884–97.
3. Hao J, et al. (2007) Interactive effects of age and estrogen on cognition and pyramidal neurons in monkey prefrontal cortex. *Proc Natl Acad Sci U S A* 104(27):11465–70.
4. Dumitriu D, et al. (2010) Selective Changes in Thin Spine Density and Morphology in Monkey Prefrontal Cortex Correlate with Aging-Related Cognitive Impairment. *J Neurosci* 30(22):7507–7515.
5. Schafer DP, et al. (2012) Microglia Sculpt Postnatal Neural Circuits in an Activity and Complement-Dependent Manner. *Neuron* 74(4):691–705.